A simplified model for frictionally dominated tidal flows

T. Van Oyen,[1] S. Lanzoni,[2] A. D'Alpaos,[3] S. Temmerman,[4] P. Troch,[1] and L. Carniello[2]

Received 9 April 2012; revised 23 May 2012; accepted 25 May 2012; published 22 June 2012.

[1] The response of vegetated tidal wetlands to environmental changes is governed by vegetation-flow-landscape feedbacks occurring over large spatial and temporal scales, and thus typically studied using simplified models. Here, we present a new simplified approach to describe frictionally dominated tidal flows, characteristic of tidal wetlands. The derivation of the model follows from an expansion of the momentum and mass conservation equations in terms of small dimensionless parameters, which arise once the relevant variables are suitably scaled. A comparison with a full-fledged finite element model indicates that the proposed simplified approach ensures a reliable description of the flow field; suggesting that the model provides a key advancement to study the bio-morphodynamic feedbacks which shape intertidal landscapes. **Citation:** Van Oyen, T., S. Lanzoni, A. D'Alpaos, S. Temmerman, P. Troch, and L. Carniello (2012), A simplified model for frictionally dominated tidal flows, *Geophys. Res. Lett.*, *39*, L12403, doi:10.1029/2012GL051949.

1. Introduction

[2] Large parts of the world's coastline are fringed by vegetated tidal wetlands such as mangroves and salt marshes [e.g., *Augustinus*, 1995; *Allen*, 2000]. These ecosystems are considered among the most valuable on earth [*Costanza et al.*, 1997]. Yet, their existence is presently challenged by climate change (relative sea-level rise, global warming) and human interference (e.g., reduced sediment supply), which may lead to drowning and large-scale die-off of tidal wetland vegetation [e.g., *Carniello et al.*, 2009; *Blum and Roberts*, 2009]. Modeling efforts provide a valuable tool to assess the vulnerability of these coastal features to external disturbances [*D'Alpaos et al.*, 2007; *Kirwan et al.*, 2010; *Fagherazzi et al.*, 2012]. These models, however, need to rely on simplified approaches [e.g., *Rinaldo et al.*, 1999] since: i) wetland dynamics are controlled by complex interactions between hydrodynamics, sediment transport and vegetation [*D'Alpaos et al.*, 2007; *Kirwan and Murray*, 2007], ii) the morphological features occur on large spatial domains ($\sim\mathcal{O}(10^3$ ha)), and iii) evolve over long timescales ($\sim\mathcal{O}$(100 years)), prohibiting the use of full numerical models.

[3] Salt marshes and mangroves have in common that the flow field on the intertidal surface is dominated by vegetation-induced friction and generated by tidal wave propagation [*Mazda et al.*, 2005; *D'Alpaos et al.*, 2007]. Presently, the most widely used model to describe the frictionally dominated hydrodynamics on the floodplain of wetlands was formulated by *Rinaldo et al.* [1999]. The model was introduced to evaluate drainage directions [e.g., *Rinaldo et al.*, 1999; *Marani et al.*, 2003] and, subsequently, used to describe the formation of channel networks in tidal marshes [e.g., *Fagherazzi and Sun*, 2004], and to model the eco-morphological evolution of tidal salt marshes [e.g., *D'Alpaos et al.*, 2007; *Kirwan and Murray*, 2007].

[4] Despite the success of the model (see *Fagherazzi et al.* [2012] for a recent review), the approach is limited since, considering a spatially uniform friction coefficient, it predicts a unique value of the flow velocity independent of the friction coefficient. To illustrate this limitation, let us recall that *Rinaldo et al.*'s [1999] approach in one horizontal (x-) direction yields (see *Rinaldo et al.* [1999] for a complete discussion of the assumptions):

$$u = -\frac{\epsilon\chi^2(\xi - z_b)}{\gamma\lambda}\frac{\partial\varsigma}{\partial x} \quad \text{and} \quad \frac{\partial^2\varsigma}{\partial x^2} = \frac{\gamma\lambda}{r\epsilon\chi^2(\xi - z_b)^2}\frac{\partial\xi}{\partial t}. \tag{1}$$

These equations are complemented by imposing a no flux boundary condition at the watershed divide ($x = L_{end}$) and $\varsigma = 0$ at the boundary between the channel and the platform ($x = 0$). In (1), u is the depth-averaged flow velocity, λ is an effective friction coefficient and z_b the floodplain bed elevation. Moreover, ϵ, r and γ are dimensionless parameters specified below and χ a Chezy friction coefficient. The variables ξ and ς denote the spatially averaged tidal elevation and the variation of the free surface from the mean, respectively. Integrating the right relation in (1) over x, taking into account the boundary conditions, we obtain

$$\frac{\partial\varsigma}{\partial x} = \frac{\gamma\lambda}{r\epsilon\chi^2(\xi - z_b)^2}\frac{\partial\xi}{\partial t}(x - L_{end}). \tag{2}$$

By re-substituting (2) into the left equation of (1), it readily follows that u is independent of the combined friction coefficient $f_r = \lambda/\chi^2$. In addition, it turns out that $u \propto (\xi - z_b)^{-1}$ such that, when ξ approaches the bed level, *Rinaldo et al.*'s [1999] approach tends to provide unreasonably large flow velocities.

[5] Here, we derive a new simplified model that can reasonably describe the flow field on the floodplain during the entire part of the tidal cycle in which the platform is flooded, and is able to account for the effect of friction. The approach follows from an analysis of the magnitude of the different terms in the momentum balance; expanding subsequently the momentum and mass conservation equations in terms of the resulting small parameters. A comparison with a full-fledged finite element model illustrates the model's capability to

[1]Department of Civil Engineering, Ghent University, Ghent, Belgium.
[2]Dipartimento di Ingegneria Civile e Ambientale, University of Padua, Padua, Italy.
[3]Department of Geosciences, University of Padua, Padua, Italy.
[4]Ecosystem Management Research Group, University of Antwerpen, Antwerpen, Belgium.

Corresponding author: T. Van Oyen, Department of Civil Engineering, Ghent University, Technologiepark 904, B-9052 Ghent, Belgium. (tomas.vanoyen@ugent.be)

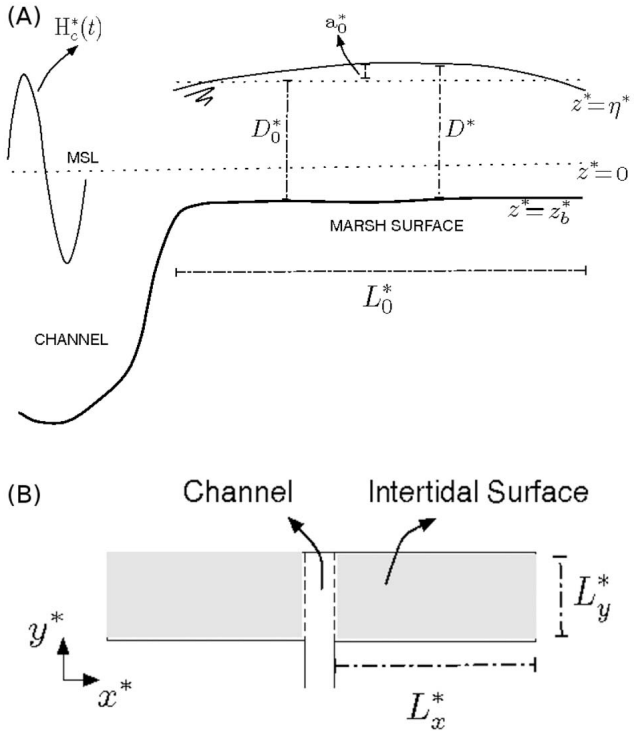

Figure 1. (a) Sketch of a typical transect perpendicular to the axis of the tidal channel flanked by a wetland. (b) Geometry of the tidal basin utilized to compare the present approach with the models of *Defina* [2000] and *Carniello et al.* [2011].

provide a reliable description of the flow field, consistent with the purpose of simulating the long-term eco-morphodynamic evolution of tidal environments.

2. Simplified Model and Solution Procedure

[6] The flow field on an intertidal platform is described by the depth-averaged hydrostatic equations of momentum and mass balance [e.g., *Dronkers*, 1964], which, in dimensionless form, read

$$\alpha\left(\frac{\partial \boldsymbol{u}}{\partial t}+r(\boldsymbol{u}\cdot\nabla)\boldsymbol{u}\right)=-\epsilon\nabla\varsigma-\frac{\gamma\lambda}{\chi^2 D}\boldsymbol{u},$$
$$\frac{d\xi}{dt}+\epsilon\frac{\partial\varsigma}{\partial t}+r\nabla\cdot(D\boldsymbol{u})=0. \quad (3)$$

The depth-averaged velocities $\boldsymbol{u}^* = (u^*, v^*)$ are scaled with U_0^*, the local depth D^* and the free surface elevation η^* by D_0^*, the horizontal directions (x^*, y^*) with L_0^* and the time t^* by the angular frequency of the tide ω^*. The quantities U_0^*, D_0^* and L_0^* denote the typical flow velocity, depth and length scales, respectively. Hereinafter, variables with (without) '*' represent dimensional (dimensionless) quantities. In equation (3), the free surface elevation $\eta(x, t)$ is split in a part independent of space $\xi(t)$ and a part which represents the spatial variations of the free surface elevation $\varsigma(x, t)$, at a given time. Here, it is important to note that the variations of η^* with respect to ξ^* do not scale with D_0^*, but, in general, are smaller; i.e., of amplitude a_0^* (see Figure 1a). The ratio between a_0^* and D_0^* is denoted by the dimensionless parameter ϵ. Friction is modeled using a Chezy friction coefficient $\chi^* = \chi_0^*\chi$ (with χ_0^* a characteristic value for the Chezy coefficient) and is linearized introducing a parameter λ. The value of the dimensionless parameter λ can be determined following the energy criterion first introduced by *Lorentz* [1926] or can be considered as a function of the local flow field to mimic non-linear friction. Future studies, focusing on the impact of vegetation on the flow field in tidal wetlands, could adopt the presented model by relating the Chezy coefficient to the local biomass as suggested by, e.g., *Baptist et al.* [2007] and *Mudd et al.* [2010]. Finally, the dimensionless parameters appearing in equations (1) and (3) are given by

$$\epsilon=\frac{a_0^*}{D_0^*},\quad \alpha=\frac{U_0^*\omega^* L_0^*}{g^* D_0^*},\quad r=\frac{U_0^*}{\omega^* L_0^*},\quad \gamma=\left(\frac{U_0^*}{\chi_0^* D_0^*}\right)^2 L_0^*. \quad (4)$$

Considering a typical value for χ_0^* and characteristic length and velocity scales on the tidal marsh platform (see Table 1), it turns out that $\alpha(\sim \mathcal{O}(10^{-3}))$ and $\epsilon(\sim \mathcal{O}(10^{-2}))$ are much smaller than $r(\sim \mathcal{O}(1))$ and $\gamma(\sim \mathcal{O}(10^{-1}))$. This motivates us to expand the solution $S = (u, v, \varsigma)$ in terms of the small parameters α and ϵ such that

$$S = S_0 + \epsilon S_{11} + \alpha S_{12} + \epsilon^2 S_{21} + \epsilon\alpha S_{22} + \alpha^2 S_{23} + \epsilon^3 S_{31} + h.o.t., \quad (5)$$

where *h.o.t.* denotes the higher order terms. Here, it is worthwhile to note that, even though ϵ is small throughout a large portion of the tidal cycle, it increases as the mean water depth decreases. Hence, for small depths, expansion (5) formally does not hold any longer and we can expect the model performance to be limited in this case. Moreover, we remark that the introduced scaling is suitable for frictionally dominated tidal flows and is therefore applicable to the (intertidal) platforms of wetlands. However, within the channels, the influence of convective and inertia terms is stronger such that expansion (4), strictly speaking, cannot be applied. Therefore, following *Rinaldo et al.* [1999], an instantaneous propagation of the tidal wave is assumed in the channels. Thus, investigating the long-term evolution of the wetland, care should be taken to possible shifts in the domain from platform regions into channels and vice versa.

[7] Substituting (5) into (3), at the leading order of approximation, the momentum conservation equations yield $\gamma\lambda\boldsymbol{u}_0/(\chi^2 D_0) = 0$, while from mass conservation, we obtain $d\xi_0/dt = 0$. It follows that $\boldsymbol{u}_0 = 0$ and ξ_0 does not depend on t.

[8] At the first order of approximation, from the momentum balance, we find that the flow field at $\mathcal{O}(\epsilon)$ is related to the gradient of local free surface variations:

$$u_{11}=-\frac{\chi^2 D_0}{\gamma\lambda}\frac{\partial\varsigma_0}{\partial x},\quad v_{11}=-\frac{\chi^2 D_0}{\gamma\lambda}\frac{\partial\varsigma_0}{\partial y}. \quad (6)$$

Table 1. Characteristic Value for χ_0^* and Typical Length and Velocity Scales on an Intertidal Platform Subject to Microtidal Forcing[a]

χ_0^*	U_0^*	L_0^*	D_0^*	a_0^*
10 $m^{1/3}$ s^{-1}	10^{-1} ms^{-1}	10^3 m	1 m	10^{-2} m

[a]See *Rinaldo et al.* [1999, Table A1, and references therein].

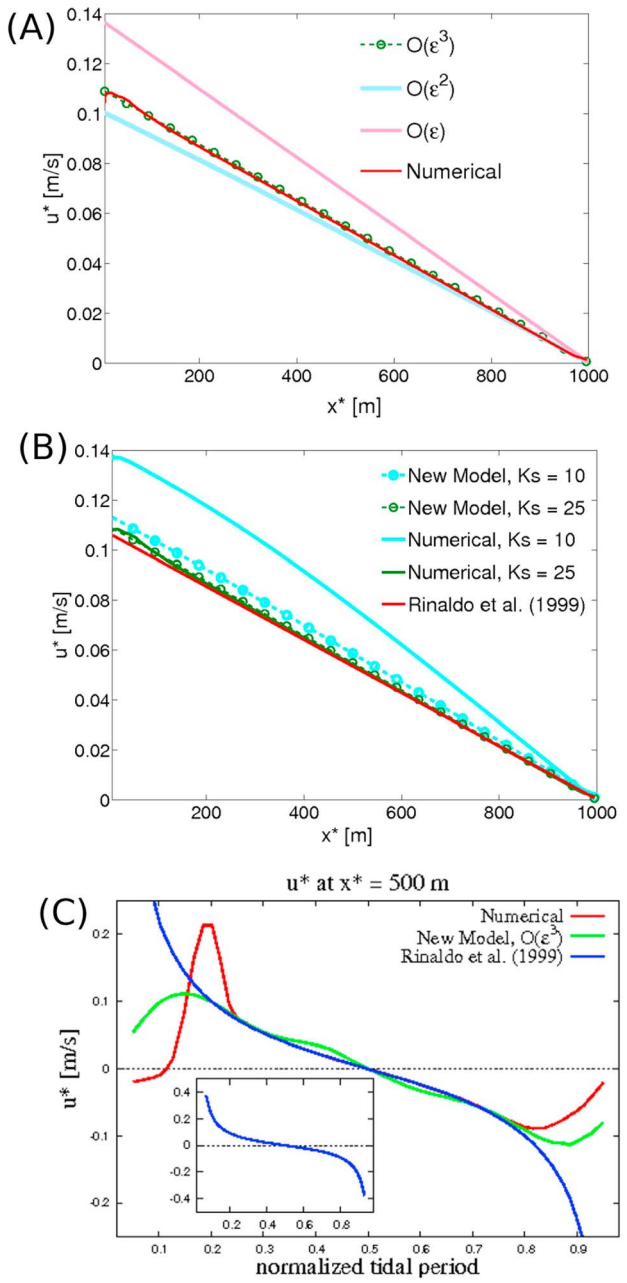

Figure 2. (a, b) Spatial distribution of the component of the velocity normal to the channel axis, along a generic transect. Figure 2a shows a comparison of the numerical solution with the present solution at the various orders of approximation for a Strickler coefficient equal to 25 $m^{1/3}$ s^{-1}. Figure 2b compares the velocity obtained through *Rinaldo et al.*'s [1999] approach, with the results of the present model and the numerical solution obtained by setting K_s^* equal to 10 and 25 $m^{1/3}$ s^{-1}. (c) The temporal variations of the velocity, obtained by the various models on the intertidal platform at a point located 500 m from the boundary between the channel and the platform. A tidal wave with amplitude of 1.0 m is considered within the channel, while the elevation z_b^* of the intertidal platform adjacent to the channel is 1 m below mean sea level. Figures 2a and 2b refer to the instant of the flooding phase at which the water level in the channel is 1.3 m.

Considering the mass balance at order ϵ and using (6), we obtain

$$\frac{d\xi_{11}}{dt} + \frac{\partial \varsigma_0}{\partial t} - r\left(\frac{\partial}{\partial x}\left[\frac{(\chi D_0)^2}{\gamma\lambda}\frac{\partial \varsigma_0}{\partial x}\right] + \frac{\partial}{\partial y}\left[\frac{(\chi D_0)^2}{\gamma\lambda}\frac{\partial \varsigma_0}{\partial y}\right]\right) = 0. \tag{7}$$

In equation (7), apparently, two unknowns arise; namely ξ_{11} and ς_0. However, the tidal wave which drives the flow field can be linked to ξ such that we can set $H_c^*(t) = D_0^*(\xi_0 + \epsilon\xi_{11})$. Here, as illustrated in Figure 1a, $H_c^*(t)$ denotes the free surface elevation of the tidal wave in the channel adjacent to the floodplain. Equation (7) is closed by imposing a no flux condition at the watershed divide and $\varsigma_0 = 0$ at the intersection between the channel and the intertidal platform. A relation similar to equation (7) was also obtained by *Friedrichs and Madsen* [1992] with a different approach; i.e., by neglecting inertial and advection terms in the momentum equations and assuming a time-invariant diffusion coefficient. Once equation (7) is solved (numerically, using a finite difference discretization), $\boldsymbol{u}_{11}$ is readily computed using relation (6). In the auxiliary material, we present the details of the higher order contributions.[1]

3. Results and Discussion

[9] To evaluate the performance of our simplified model, we compare the resulting flow field with that obtained from a full-fledged finite element model [*Defina*, 2000; *Carniello et al.*, 2011]. In order to facilitate the comparison, a simplified domain is considered (see Figure 1b); in particular, the domain consists of one short channel flanked by two horizontally symmetric tidal flats. Results considering a realistic geometry based on the San Felice salt marsh, observed in the Venice Lagoon (Italy), are presented in the auxiliary material. In the numerical model, the free surface elevation of the tidal wave is imposed within the channel of the schematic basin. The width L_x^* of the tidal flat in the x^*– direction is 1000 m while the length L_y^* is equal to 500 m. Owing to the short length of the tidal basin, the tidal wave is assumed to propagate almost instantaneously through the channel such that only the flow velocity in the x^*–direction is of interest, i.e., $v^* = 0$ on the tidal flat.

[10] Figure 2a shows the magnitude of the velocity u^* along a generic transect during the flooding phase, considering a tidal wave with amplitude (A_p^*) 1.0 m and a mean sea level (m.s.l.) of 1 m above the bed level z_b^*. In particular, the figure refers to the instant at which H_c^* is equal to 1.3 m. In the numerical model, friction is described with a Strickler coefficient K_s^* (in Figure 2a, K_s^* is equal to 25 $m^{1/3}$ s^{-1}). To compare the simplified with the numerical model, we relate the Chezy coefficient to K_s^*. In particular, the Chezy coefficient is set equal to $\chi^* = K_s^*(H_c^* - z_b^*)^{1/6}$, with H_c^* the free surface elevation at the considered instant. Moreover, in order to mimic non-linear friction, the value prescribed for λ at a given time is related to the local flow velocity obtained at previous time steps by setting $\lambda = \sqrt{u_{prev}^2 + v_{prev}^2}$ with $\boldsymbol{u}_{prev}$ the local flow velocity averaged over two previous time steps. From Figure 2a, it appears that the simplified approach

[1]Auxiliary materials are available in the HTML. doi:10.1029/2012GL051949.

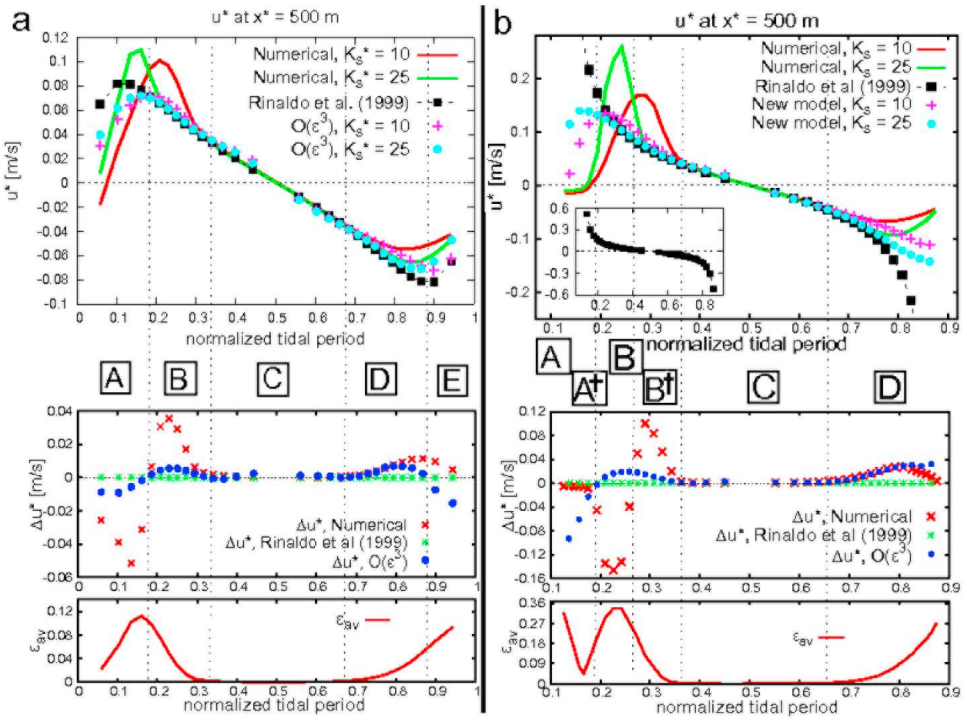

Figure 3. (a, b) Temporal variations of (top) the velocity u^* and (middle) the difference Δu^* ($\Delta u^* = u^*_{rg} - u^*_{sm}$) observed on the intertidal platform at a point located 500 m from the boundary between the channel and the platform (i.e., near to the watershed divide) for two different values of the Strickler coefficient (K_s^* = 10 and 25 $m^{1/3}$ s^{-1}). (bottom) The variation of the value of ϵ_{av} during the tidal cycle is illustrated in the case K_s^* is 10 $m^{1/3}$ s^{-1}. The variable ϵ_{av} is the spatially averaged (over the entire transect) value of the parameter ϵ. The latter is evaluated using the free surface elevation obtained by the numerical model. In Figure 3a, a tidal wave with amplitude of 0.75 m and a mean sea level of 1.0 m above z_b^* is considered while Figure 3b illustrates the results for an amplitude of 1 m and a mean sea level of 0.75 m above z_b^* (thus implying that the intertidal platform dries during ebb). Several regions are indicated in the top and middle panel (denoted by A, A†, B, B†, C and D), the significance of which is explained in the main text.

describes the flow velocity reasonably well, and that the solution improves if higher order contributions are taken into account. Similar results are obtained considering different instants of the tidal cycle, except at low tide, near flow reversal, when the depth is small. Note that only the flow velocities at $\mathcal{O}(\epsilon)$, $\mathcal{O}(\epsilon^2)$ and $\mathcal{O}(\epsilon^3)$ are shown since the contributions to u^* of the orders α and α^2 are identically zero and the influence of $\mathcal{O}(\epsilon\alpha)$ turns out to be negligible.

[11] In Figure 2b, a comparison is presented of the flow velocity along a generic transect obtained with *Rinaldo et al.*'s [1999] approach, the present model and the numerical solution considering K_s^* equal to 10 and 25 $m^{1/3}$ s^{-1}; while Figure 2c illustrates the variation of u^* in time, on the intertidal platform at a distance of 500 m from the boundary between the channel and the platform. Figure 2b shows that the model of *Rinaldo et al.* [1999], at the considered instant, reasonably describes the main features of the flow field [*Marani et al.*, 2003]. However, that model cannot account for variations of the spatially uniform friction coefficient, while the present approach, similar to the numerical model, leads to larger flow velocities for K_s^*= 10 $m^{1/3}$ s^{-1} than for K_s^*= 25 $m^{1/3}$ s^{-1}; even though the discrepancy between the numerical and the present model, at this instant, is large in the former case. Moreover, Figure 2c shows that, even though the proposed model is formally not valid for small depths, the errors associated with the estimated velocity under these conditions are much smaller than those resulting from *Rinaldo et al.*'s [1999] approach. In particular, the new model provides a finite velocity field for small depths, while *Rinaldo et al.*'s [1999] model loses its validity when the water depth tends to zero.

[12] To investigate the capability of the present model to properly account for friction effects, considering a spatially uniform friction coefficient, in the upper plots of Figures 3a and 3b, we show the temporal variations of u^* at a location 500 m from the boundary between the flat and the channel, considering different friction coefficients (K_s^* = 10 and 25 $m^{1/3}$ s^{-1}). In addition, the middle plots of Figures 3a and 3b show the difference Δu^* between the flow velocity when K_s^* is 10 $m^{1/3}$ s^{-1} (u^*_{rg}) and when K_s^* is set 25 $m^{1/3}$ s^{-1} (u^*_{sm}), i.e., $\Delta u^* = u^*_{rg} - u^*_{sm}$. A higher (lower) value of χ^* or K_s^* relates to less (more) friction. In Figures 3a and 3b, we consider a tidal wave with different amplitudes and mean sea level, to analyze the model performance in case the platform falls dry during a period of the ebb tide (Figure 3b, A_p^* = 1 m, m.s.l. = 0.75 m above z_b^*); and when the platform is always submerged (Figure 3a, A_p^* = 0.75 m, m.s.l. = 1 m above z_b^*).

[13] Several regions can be recognized in Figure 3. In the region A (A†), characterized by the flow field acceleration during the initial flooding phase, both the numerical and the simplified model indicate that the velocity towards the

watershed divide attains larger values when the friction is lower. This initial phase of the flooding is also characterized by a peak velocity, related to the run-up of the tidal wave on the platform. Figures 2c, 3a, and 3b show that the present model underestimates u^* at this instant, even though, it still provides a reasonable description. Note that, as illustrated in the lower panel of Figures 3a and 3b, at this instant an increase in the value of ϵ occurs. In region B ($B^\dagger$), the velocities decrease and u^*_{rg} becomes larger than u^*_{sm}, for both the numerical and the simplified model. Here, it is worth to remark that when the water level falls below z^*_b during the ebb phase (Figure 3b), a phase shift in time between the boundaries of the regions A ($A^\dagger$) and B ($B^\dagger$), predicted by the simplified and numerical model, is found. The regions with (without) '†' correspond to the numerical (simplified) results, when the regions do not coincide. This occurs because the numerical model also accounts for inertia effects and, hence, it takes a certain amount of time for the tidal wave to propagate from the channel to a certain point on the tidal flat; while the simplified model assumes the instantaneous propagation of the mean tidal level (ξ) on the tidal flat. Moreover, according to the numerical model, u^* is not identical to zero at the beginning of the flood phase (Figure 3b); since, even though H^*_c is below z^*_b, some water has still to be drained from the floodplain. In the region C, the velocity and Δu^* almost vanish, since the tide is reversing. Next, the flow accelerates again into the channel (ebb phase, region D) and the amplitude of u^*_{sm} is found (both for the simplified and numerical model) larger than that of u^*_{rg}. Finally, Figure 3a shows the presence of a region (E), near to low tide, where Δu^*, although attaining different values in the numerical and the simplified models, progressively decreases. Similar results are obtained for smaller values of L^*_x, even though the magnitude of Δu^* tends to decrease.

[14] Hence, the results show that the simplified approach provides a reliable description of the flow field on the intertidal platforms, also accounting for the influence of friction. Clearly, some differences occur with respect to the complete numerical model, in particular shortly before and after low tide. Indeed, during this phase of the tidal cycle, as illustrated by the lower panels of Figures 3a and 3b, ϵ is no longer a small variable; reflecting thus a limitation of the model related to expansion (5) which, strictly speaking, does not hold for small depths and during the run-up of the tidal wave on the tidal platform. Nevertheless, it appears that the introduced approach meets the objective of this study; which is not to describe accurately the flow field, but to provide a model that can be applied in long-term studies on the eco-geomorphic response of tidal wetlands.

4. Conclusions

[15] A simplified approach is proposed to describe frictionally dominated tidal flows that is able to account for the influence of friction, and can be used for long-term simulations of the eco-geomorphic evolution of tidal wetlands. The model is based on an expansion of the depth-averaged momentum and mass balance, in the small parameters appearing after suitably scaling the relevant variables. A comparison between the simplified model and a numerical model that solves the complete two-dimensional shallow water equations shows that, even though some differences are present, the introduced approach provides a reliable description of the flow field, capturing also the affects of bed friction variability. This is a key issue when considering the eco-morphologic evolution of tidal wetlands. The presence of vegetation, in fact, strongly affects flow resistance and, hence, the velocity field which, in turn, controls sediment and nutrient dynamics. Even though the model could be further improved, e.g., by accounting for the wetting-drying process and by relaxing the assumptions of i) the small value of ϵ and ii) an instantaneous propagation in the channels, we deem that the present model provides a valuable tool for the broader scientific community studying the ecology and geomorphology of vegetated tidal landscapes.

[16] **Acknowledgments.** The first author wishes to acknowledge the Ghent University (Special Research Fund) for his post-doctoral grant. The research has been partially stimulated by the Scientific Research Community: "The functioning of river ecosystems through plant-flow-soil interactions". Partial funding has been provided by MIUR within the project PRIN 2008, "Eco-morphodynamics of tidal environments and climate change." and by the University of Padua, within the project "Morphodynamics of marsh systems subject to natural forcings and climate changes". The paper greatly benifited from a thorough review by Sergio Fagherazzi and from a discussion with Huib de Swart.

[17] The Editor wishes to thank Sergio Fagherazzi for assisting in the evaluation of this paper.

References

Allen, J. R. L. (2000), Morphodynamics of Holocene salt marshes: A review sketch from the Atlantic and southern North Sea coasts of Europe, *Quat. Sci. Rev.*, *19*, 1155–1231.

Augustinus, P. G. E. F. (1995), Geomorphology and sedimentology of mangroves, in *Geomorphology and Sedimentology of Estuaries*, edited by G. M. E. Perillo, 333–357, Elsevier, Amsterdam.

Baptist, M. J., Babovic, V., Uthurburu, J. Rodriguez, M. Keijzer, R. E. Uittenbogaard, A. Mynett, and A. Verwey (2007), On inducing equations for vegetation resistance, *J. Hydraul. Res.*, *45*(4), 435–450.

Blum, M. D., and H. H. Roberts (2009), Drowning of the Mississippi Delta due to insufficient sediment supply and global sea-level rise, *Nat. Geosci.*, *2*, 488–491, doi:10.1038/ngeo553.

Carniello, L., A. Defina, and L. D'Alpaos (2009), Morphological evolution of the Venice lagoon: Evidence from the past and trend for the future, *J. Geophys. Res.*, *114*, F04002, doi:10.1029/2008JF001157.

Carniello, L., A. D'Alpaos, and A. Defina (2011), Modeling wind waves and tidal flows in shallow micro-tidal basins, *Estuarine Coastal Shelf Sci.*, *92*, 263–276, doi:10.1016/j.ecss.2011.01.001.

Costanza, R. R., et al. (1997), The value of the world's ecosystem services and natural capital, *Nature*, *387*, 252–260.

D'Alpaos, A., S. Lanzoni, M. Marani, and A. Rinaldo (2007), Landscape evolution in tidal embayments: Modeling the interplay of erosion, sedimentation, and vegetation dynamics, *J. Geophys. Res.*, *112*, F01008, doi:10.1029/2006JF000537.

Defina, A. (2000), Two-dimensional shallow flow equations for partially dry areas, *Water Resour. Res.*, *36*(11), 3251–3264.

Dronkers, J. J. (1964), *Tidal computations in Rivers and Coastal Waters*, North-Holland, Amsterdam.

Fagherazzi, S., and T. Sun (2004), A stochastic model for the formation of channel networks in tidal marshes, *Geophys. Res. Lett.*, *31*, L21503, doi:10.1029/2004GL020965.

Fagherazzi, S., et al. (2012), Numerical models of salt marsh evolution: Ecological, geomorphic, and climatic factors, *Rev. Geophys.*, *50*, RG1002, doi:10.1029/2011RG000359.

Friedrichs, C. T., and O. S. Madsen (1992), Nonlinear diffusion of the tidal signal in frictionally dominated embayments, *J. Geophys. Res.*, *97*(C4), 5637–5650.

Kirwan, M. L., and A. B. Murray (2007), A coupled geomorphic and ecological model of tidal marsh evolution, *Proc. Natl. Acad. Sci. U. S. A.*, *104*, 6118–6122, doi:10.1073/pnas.0700958104.

Kirwan, M. L., G. R. Guntenspergen, A. D'Alpaos, J. T. Morris, S. M. Mudd, and S. Temmerman (2010), Limits on the adaptability of coastal marshes to rising sea level, *Geophys. Res. Lett.*, *37*, L23401, doi:10.1029/2010GL045489.

Lorentz, H. A. (1926), Verslag staatcommissie zuiderzee 1918–1926, technical report, Rep. Gov. Zuiderzee Comm., Alg. Landsdrukkerij, The Hague, Netherlands.

Marani, M., E. Belluco, A. D'Alpaos, A. Defina, S. Lanzoni, and A. Rinaldo (2003), On the drainage density of tidal networks, *Water Resour. Res.*, *39*(2), 1040, doi:10.1029/2001WR001051.

Mazda, Y., D. Kobashi, and S. Okada (2005), Tidal-scale hydrodynamics within mangrove swamps, *Wetlands Ecol. Manage.*, *13*, 647–655, doi:10.1007/s11273-005-0613-4.

Mudd, S. M., A. D'Alpaos, and J. T. Morris (2010), How does vegetation affect sedimentation on tidal marshes? Investigating particle capture and hydrodynamic controls on biologically mediated sedimentation, *J. Geophys. Res.*, *115*, F03029, doi:10.1029/2009JF001566.

Rinaldo, A., S. Fagherazzi, S. Lanzoni, M. Marani, and W. E. Dietrich (1999), Tidal networks: 2. Watershed delineation and comparative network morphology, *Water Resour. Res.*, *35*(12), 3905–3917.